

International Conference on Space Optics—ICSO 2022

Dubrovnik, Croatia

3–7 October 2022

Edited by Kyriaki Minoglou, Nikos Karafolas, and Bruno Cugny,



Interferometric Quantification and Identification of Back-reflected and Back-scattered Light from a System of Two Optical Components



Interferometric Quantification and Identification of Back-reflected and Back-scattered Light from a System of Two Optical Components

Imran Khan, Michel Lequime, Myriam Zerrad, and Claude Amra

Aix Marseille Univ, CNRS, Centrale Marseille, Institut Fresnel, Marseille, France

ABSTRACT

In this work, we recorded the retro-reflected and back-scattered light from a system of two components i.e, a single side AR coated SiO₂ window and a mirror placed at tilt angle of 10° in the transmission of the window. Retro-reflection and back-scattering from components in an optical system can be detrimental for system performance such as the phase measurement errors, ghost images and laser induced damage in gravitational wave interferometry, optical communications, biomedical imaging and high power laser systems, respectively. Therefore, an accurate determination of the retro-reflected and back-scattered light in such systems is imperative for optimized system performance, particularly the systems where extreme phase sensitive measurements are of keen interest such as the gravitational wave detectors LIGO, Virgo, KAGRA, the future planned Einstein Telescope (ET) and Laser Interferometer Space Antenna (LISA). Using a balanced optical low coherence interferometer, we recorded and distinguished the contribution of light retro-reflected and back-scattered from the different optical surfaces of the two-component assembly. This work would pave the way for simultaneous characterization of the spectral properties of light retro-reflected and back-scattered by components in an optical system with the capability to accurately and effectively identify the impact of individual components as well as the global system performance.

Keywords: Back-scattered light, Low coherence interferometry, Gravitational wave detectors

1. INTRODUCTION

Scattered light characterization of optical components is critical to assess the design performance of many optical systems such as large size optical telescopes, interferometers, imaging and detection systems, where scattered light can degrade the desired detection sensitivity and induce ghost images. In particular, the high precision optical systems such as the laser interferometry based gravitational wave (GW) detectors,¹⁻³ where the phase of the output light field provides insight into the nature of the astrophysical sources that radiate energy as gravitational waves upon their interactions with the space-time continuum. The LIGO-Virgo observatories have opened this new window on observational astronomy and have provided exciting insights into some of the extreme astrophysical interactions such as binary system of black holes, neutron stars and systems consisting of a black hole and a neutron star. And, the future planned GW observatories such as the LISA mission by European space agency (ESA) and Einstein telescope (ET) will further enhance the capability of laser interferometry based gravitational wave detections in the lower detection bandwidth i.e, 0.1 mHz to 10 Hz.⁴⁻⁷

The interferometric detection of gravitational waves require extreme operating conditions to overcome many instrument noise sources and one such noise is the stray light that can induce phase measurement errors, thus limiting the ultimate system performance. In the case of LISA interferometer, the phase uncertainties on the order of a few microradians can be induced by ultra-weak retroreflected or back-scattered light in the output signal, with relative power of about 10⁻¹² and therefore need careful attention and consideration.⁷⁻¹³

And in that context, we used a low coherence interferometer with balanced detection scheme that allows the suppression of the relative intensity noise of the light source and thus unlock greater detection sensitivity as such that very tiny amount of back-scattered light from an optical component can be accurately recorded.

Further author information: (Send correspondence to Imran Khan)
E-mail: imran.khan@fresnel.fr

The use of a low coherence interferometer also allows to distinguish the contribution of back-reflected and back-scattered light from the different optical interfaces involved in the measurement and which is quite useful for systems comprising of multiple optical components, where individual as well as the global system performance can be evaluated. In our previous demonstrations, we have achieved the measured back-reflectance^{14–17} from N-BK7, S-LAH66 windows and a Silver coated mirror (angular dependence of back-reflectance in this case) on the order of 10^{-10} where the sample consists of a single component only. Now, we have extended the capability of our measurement system to record the back-reflected and back-scattered light from a system of two optical components, simultaneously. As is the case of LISA optical bench, where multiple optical components comprising of beam splitters, telescope, photodiodes and beam dumps, it can be an important consideration to have the global system performance of the optical board in terms of back-scattered light along with the individual component level performance. And therefore, we present our preliminary demonstration of the back-scattered light recorded from a sample assembly that consists of an anti-reflection coated optical window and a mirror placed in the transmission of the window.

2. THEORETICAL DISCUSSION

For a input light source whose spectral shape is given by Gaussian beam profile $\frac{P_0}{\delta f \sqrt{\pi}} e^{-\left[\frac{f-f_0}{\delta f}\right]^2}$, a low coherence interferometer provides the following output signal^{14–18} as a result of the interfering beams from the sample and the reference arms.

$$V(t) = G\mathcal{T} \Re \left\{ \int_0^\infty S(f)\mathcal{P}(f)r(f)e^{-\iota k\Delta L} df \right\} \quad (1)$$

Where G is the transimpedance gain of the photoreceiver, $S(f)$ is the responsivity of the photoreceiver, $\mathcal{P}(f)$ is the input light source power spectrum, $r(f)$ is the surface reflectivity of the sample, k is source wavenumber, ΔL is the optical path length difference between the sample and the reference arm of the interferometer, and \mathcal{T} is

$$\mathcal{T} = 2\eta_\alpha \left(\sqrt{T_{ref,1}T_{sig,1}} + \alpha \sqrt{T_{ref,2}T_{sig,2}} \right) \quad (2)$$

where $T_{REF,j}$ and $T_{SIG,j}$ ($j = 1, 2$) are the transmission coefficients of the reference and signal arms, respectively, α is a coefficient corresponding to the fine tuning of the balance between the two detection channels, η_α is detection efficiency [$\eta_\alpha = 1 - e^{(-2a^2/w_d^2)}$] with $2a$ the photodiode diameter and $2w_d$ that of the gaussian beam on the photodiodes. For a multi surface optical sample, equation 1 can be written as

$$V(t) = G\mathcal{T} \Re \left\{ \int_0^\infty S(f)\mathcal{P}(f)r_1(f)e^{-2\iota\pi\frac{2v}{c}f} df \right\} + G\mathcal{T} \Re \left\{ \int_0^\infty S(f)\mathcal{P}(f)r_2(f)e^{-2\iota\pi\frac{2[vt-n_s(f)d_s]}{c}f} df \right\} + \dots \quad (3)$$

where v is the translation speed of the reference mirror, n_s is the sample refractive index, d_s is the sample geometrical thickness, and c is the speed of light. We can re-write $V(t)$ as the time dependent voltage signal recorded from the interfaces of an optical window as

$$V(t) \approx V_1(t) + V_2(t) + \dots \quad (4)$$

$V_1(t)$ and $V_2(t)$ are signals from the front face with coefficient of reflection $r_1(f)$ and the rear face with coefficient of reflection $r_2(f)$ of the window which are acquired using a balanced photoreceiver. The use of balanced photo detection in optical systems lead to the suppression of the common noise thus allowing the detection of small differences in optical powers of the input signals. The two optical fields from the reference and sample arms are overlapped on a 50:50 beamsplitter and recorded by two identical photodiodes. In this way, the two photodiodes generate the photocurrents comprised of DC and AC parts given by

$$\begin{aligned} I_1 &= I_{DC,1} + I_{AC,1} \\ I_2 &= I_{DC,2} - I_{AC,2} \end{aligned} \quad (5)$$

These generated photocurrents are electronically subtracted and the amplified differential output voltage signal is provided to the DAQ module, so actually, equation 4 is

$$V(t) = G(I_{AC,1} - \alpha I_{AC,2}) = G(I_{AC,1} - \cos^2 \beta I_{AC,2}) \quad (6)$$

where β is the rotation of the linear polarizer LP_1 (in Fig. 1), used for fine tuning the balancing of optical power on the two photodiodes. The reference arm of a low coherence interferometer is translated to record the signals from the different interfaces of a given sample as a function of the optical path difference between the reference and signal arms ($\Delta L = 2vt$) and the resulting signal is called an echo or an interferogram.

$$\Delta L = L_R - L_S = 2(z_R - z_S) \quad (7)$$

where z_R and z_S are the optical path lengths of the reference and signal arms, respectively. The width of the interferogram or echo is defined by the coherence length l_c and the central wavelength of the input light source.

$$l_c = \frac{1}{\pi\delta f} = \frac{2\sqrt{\ln(2)}}{\pi} \frac{\lambda_0^2}{\Delta\lambda} \quad (8)$$

3. THE EXPERIMENT

The optical layout of the experiment is shown in Fig.1. A linearly polarized 60 mW pigtailed superluminescent diode (SLD) source with a central wavelength (λ_0) of 1060 nm and FWHM bandwidth of 70 nm is used to illuminate the interferometer. The pigtail consists of a PMF 980-XP single mode fiber whose output is located in the focal plane of a reflective collimator (FC) with an effective focal length of 7 mm thus providing a Gaussian collimated light beam with a waist diameter around 2 mm. Using a 50:50 cube beam splitter (BS1), the input optical beam is split into the signal and reference arms of the interferometer and the input state of polarization is controlled using the linear polarizer LP_0 . The sample assembly that consists of a single side anti-reflection coated (ARCW) Silica (SiO_2) window mounted on (Newport RGV100BL-S) stage and a mirror (M_6) placed in the transmission of the window at tilt angle (θ_{tilt}), is illuminated by the reflected beam from cube beam splitter BS1. The transmitted beam through BS1 is retro-reflected from a hollow retro-reflector (HRR) mounted on Newport XMS-100 S motorized linear translation stage and together with a right angle prism (RAP) is directed onto the cube beam splitter BS2. The retro-reflected and back-scattered light from the sample are recombined

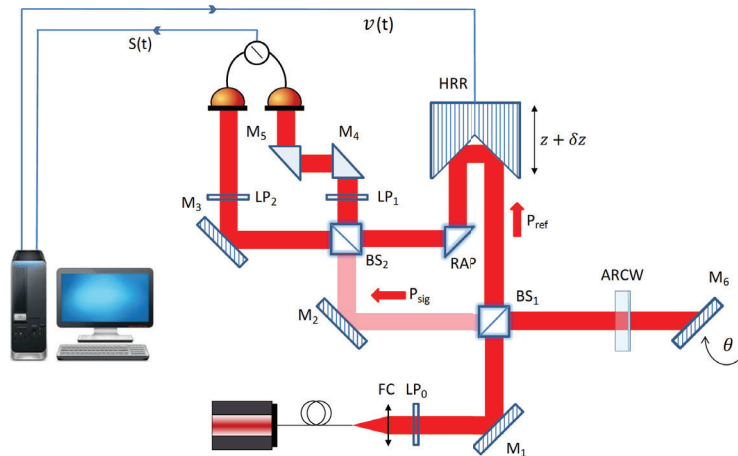


Figure 1. Optical layout. $S(t)$ is the signal recorded from the photoreceiver and the $v(t)$ is the control signal used to translate the reference mirror at a constant velocity v .

with the reference beam onto the cube beam splitter BS2 and the resulting time dependent voltage signal is recorded using a balanced photo-receiver (Newport Nirvana 2017 model). In order to match the optical paths of the two beams after the BS2, we use a periscope that is formed using mirrors M_4 and M_5 . The output channel of the balanced photoreceiver is acquired using a National Instruments (NI) data acquisition (DAQ) module USB-6361 (16 bits, 2 MS/s) and the data are post processed numerically.

4. RESULTS AND DISCUSSION

The alignment of the sample assembly is optimized as such the reflected beam is overlapped onto the reference arm beam and the resulting signal is recorded with the balanced photoreceiver. The sample that consists of a Silica ARCW is placed as such the uncoated interface is illuminated with the incident light beam and a mirror placed in tilted position is illuminated by the beam transmitted by the ARCW. In order to record a measurement, the reference arm is translated at a constant velocity to cover a displacement of 59 mm that corresponds to a total travelled distance (d_t) that is much greater than the geometrical thickness of ARCW and the distance between ARCW and the mirror.

$$d_t \gg 2 \times n_g d_s + d_M \quad (9)$$

where n_g is the group index of the ARCW and d_M is the geometrical distance between the rear face of ARCW and the mirror. The light source driving current used for the measurement is $I=190$ mA that corresponds to the non-saturated operating condition of the balanced photoreceiver and the recording of voltage signal within the ± 10 V digitization limit of the data acquisition board.

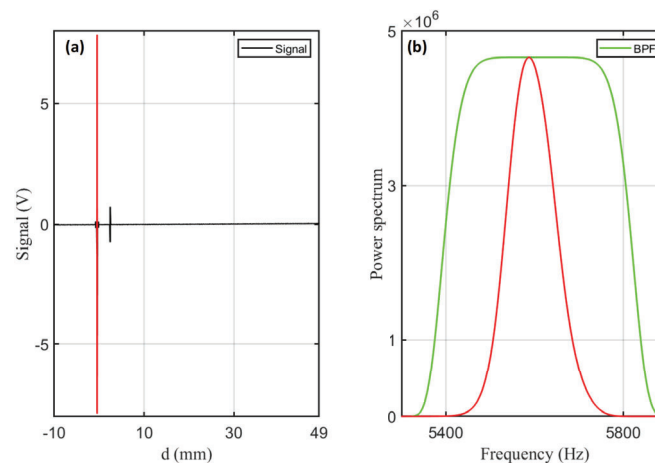


Figure 2. **a**: Recording of the time dependent voltage signal $V(t)$ as a function of the optical path difference between sample and reference arms. The reference arm is translated at a constant velocity of 3 mm/s. **b**: Band pass filter around the signal of interest defined by the translation speed of the reference arm i.e, $f_c = \frac{2v}{\lambda_0}$.

We first recorded the signal from the sample that only consists of ARCW at 0° sample tilt angle as is shown in Fig. 2 (a). The length of the scan that corresponds to the maximum distance travelled by the reference mirror is kept fixed for all the measurements onwards in order to keep the operating conditions homogeneous. The red highlighted part of the recorded data shows the back-reflected light from the uncoated front face of the ARCW and is used to define the band pass filter (BPF) centred at carrier frequency of 5.6 kHz as can be seen in Fig. 2 (b) to frequency filter the data. This carrier frequency is generated in the response of the interferometer due to the reference mirror translation at a constant velocity v .

The recorded data in Fig. 2 (a) are zoomed in by taking into account the two visible echoes that correspond to the uncoated front face (S_1) and the coated rear face (S_2) of the ARCW. The distance between these two echoes that corresponds to the geometrical thickness of the ARCW is used to compute the location of the echo (S_3) that corresponds to the first multiple reflection of the incident light beam within the window and the location of the second multiple reflection of the incident light beam that corresponds to the noise of the system as can be seen in Fig. 3. The presence of laser line anti-reflection coating on the rear face of the SiO_2 window suppresses the back-reflection of the incident light by an order of magnitude 100 as is evident between the two recorded signals S_1 and S_2 corresponding to echoes ($S_2 \sim 0.1 \times S_1$) with coefficient of reflections ($R_1 = 0.0337$ and $R_2 = 2.78 \times 10^{-4}$). And moreover, the measured coefficient of reflection corresponding to the first multiple reflection of the incident light within the ARCW echo S_3 is ($R_3 = 4 \times 10^{-9}$) which in terms of the amplitude suppression of back-reflection is ($S_3 \sim 3.5 \times 10^{-4} \times S_1$), as can be seen in Fig. 4.

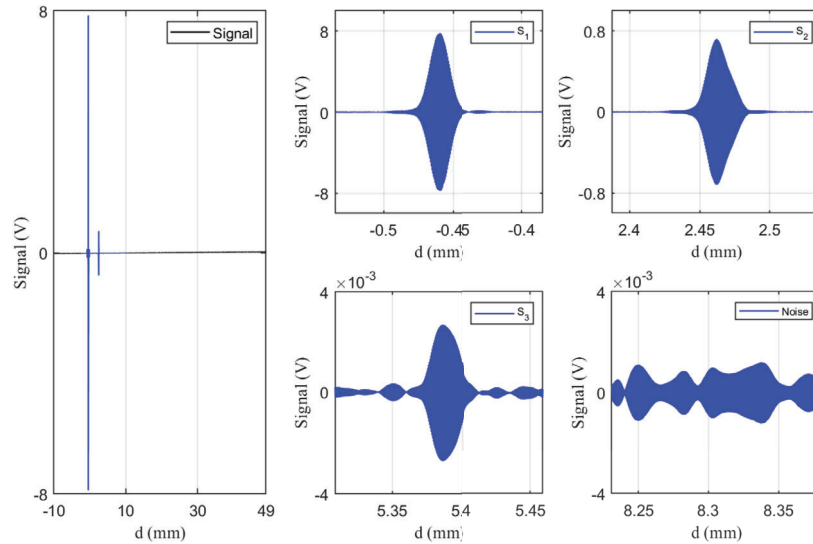


Figure 3. Long scan represents the raw data recorded from the sample. The frequency filtered individual echoes that correspond to the front face (S_1), rear face (S_2) and the first multiple reflection (S_3) within the ARCW. This measurement shows the signal recorded from the sample that consists of ARCW only.

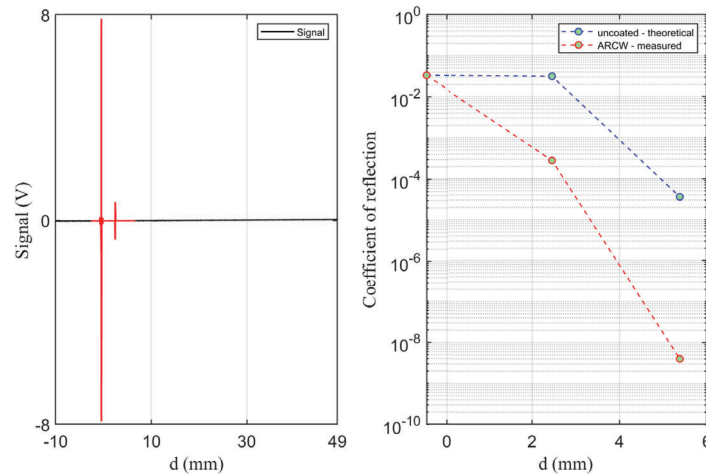


Figure 4. The signal contribution from the ARCW (shown in red color) is frequency filtered to extract the coefficient of reflection from the front face, rear face and the first multiple reflection within the ARCW. The measured coefficient of reflection are: front face ($R_1 = 0.0337$), rear face ($R_2 = 2.78 \times 10^{-4}$), and the first multiple reflection within the ARCW ($R_3 = 4 \times 10^{-9}$).

After recording the back-reflected light from the ARCW, next, we placed a mirror (M_6 in Fig. 1) in tilted position behind the ARCW to record the back-scattered light. The back-scattered light contributions from the mirror in this assembly are transmitted through the ARCW, thus are slightly attenuated by the two faces of the ARCW ($T = (1 - R_1)(1 - R_2) \sim 0.96$). We aligned this mirror M_6 by overlapping the directly reflected beam onto the interference beam between the ARCW and the reference arm. We first recorded the signals in the retro-reflection regime with small tilt angles $\theta_{tilt} < 1.5^\circ$ as is shown in Fig. 5. For every mirror tilt angle, the reference arm is displaced by 59 mm as was the case of signal recording from the ARCW only (discussed above) and the selected region from the long scan (as is shown in blue color) is the optical path length difference between the reference arm and the mirror (M_6). Fig. 5 (a) shows the recording of the signal from ARCW in the absence of the mirror and shows some spurious signals that do not correspond to the optical path difference based on the geometrical position of the ARCW and the mirror and are always present in all the measurements.

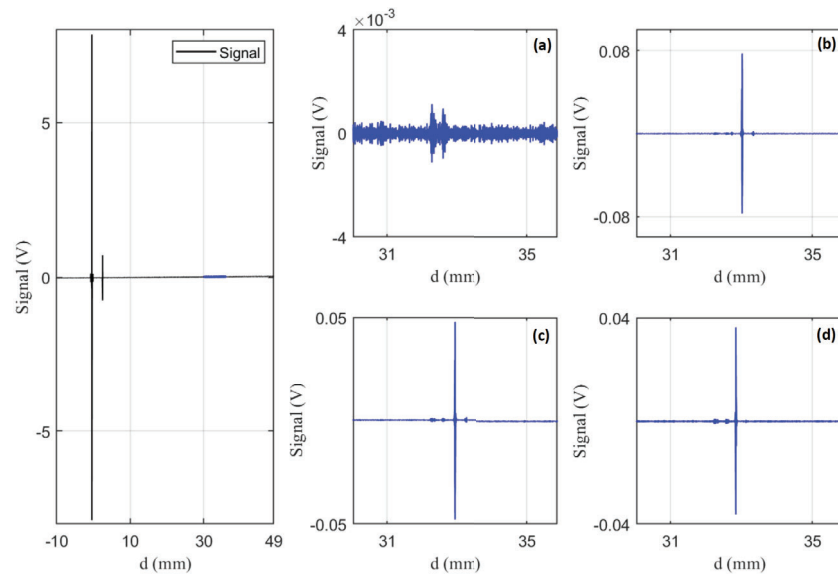


Figure 5. Part of the recorded long scan (as is indicated by blue color) that correspond to the scattered light contribution from a mirror placed behind the ARCW, thus forming a sample assembly comprising of two optical components. (a): The sample consists of ARCW only. These two tiny peaks are spurious signals that are always present regardless of the presence or absence of the mirror in the transmission of ARCW and do not correspond to the optical path difference between sample and reference arm based on their geometrical distance. (b): The sample consists of ARCW and the mirror placed at tilt angle of $< 0.5^\circ$, (c): the sample consists of ARCW and the mirror placed at tilt angle of $< 1^\circ$, and (d): the sample consists of ARCW and the mirror placed at tilt angle of $< 1.5^\circ$.

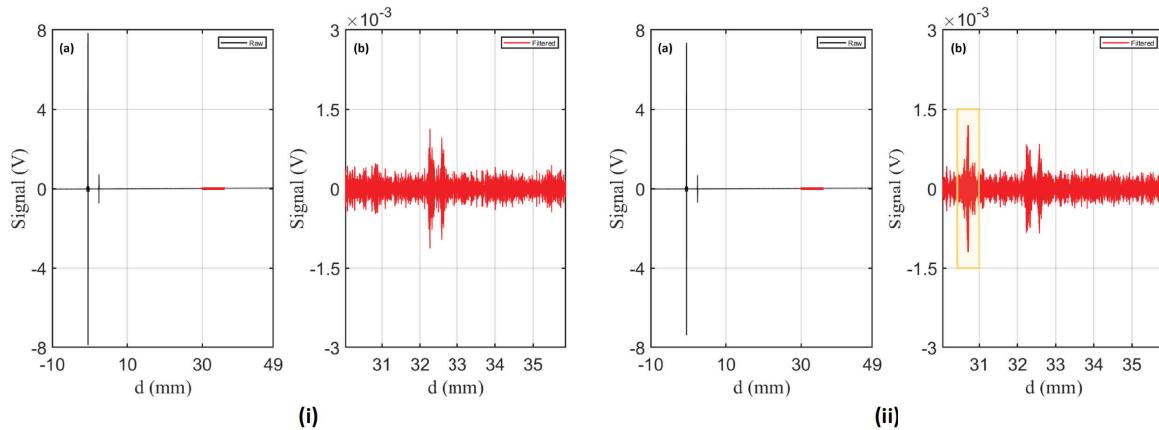


Figure 6. (i): The long scan recorded from the sample that consists of ARCW only. The red highlighted part of the signal shows the region where any scattered light contribution from the tilted mirror is expected (depending on the geometrical distance between the ARCW and the mirror). (ii): The long scan recorded from the sample that consists of ARCW and a tilted mirror placed in the transmission of ARCW. The yellow highlighted part of Fig. (ii-b) shows the scattered light recorded from the mirror at around 10° of mirror tilt angle.

Next, we rotated the mirror with small tilt angles and the corresponding signal contributions from the mirror can be seen in Fig. 5 (b, c and d). As expected, we can see that as the mirror tilt angle increases in steps, the recorded signal amplitude level decreases.

And finally, after recording the signals close to the retro-reflection regime, we recorded the back-scattered light from the mirror placed behind the ARCW with a tilt angle of around 10° as is shown in Fig. 6. Fig. 6 (a) shows the recording of the signal from sample assembly that consists of the ARCW only while Fig. 6 (b) shows

the recording of the signal from the sample assembly in the presence of the mirror tilted at an angle of 10° . The recording of this signal is of particular interest as it demonstrates the ability of our instrument to identify the position of the sources of stray light, whether reflective or diffusive, and to quantify their effective contribution (i.e. recoupled into the single-mode illumination beam).

5. CONCLUSION

In this work, we have performed the recording of the back-reflected and back-scattered light from a sample assembly of two optical components comprising of a ARCW and a mirror placed in the transmission of the ARCW. Our measurements have shown that a low coherence interferometer with balanced detection can allow the accurate recording of the back-reflected light from a ARCW to quantify the coefficient of reflection of the sample interfaces in the presence of AR coating on the substrate. Moreover, the back-scattered light is recorded from a mirror that is placed in the transmission of the ARCW, thus demonstrating the system capability of recording light scattering from a mirror that is located behind another component i.e., an ARCW. This demonstration would pave the way for stray light performance evaluation of optical systems such as the LISA optical bench where the presence of multiple components can be detrimental for stray light contribution due to the onboard high power laser source.

ACKNOWLEDGMENTS

This work is part of the StrayLight Working Group for the Laser Instrument Group of the LISA Consortium. The authors would like to thank the AMIdex Talents Management Program, Aix Marseille University and the French National Space Center (CNES) for their financial support.

REFERENCES

- [1] The LIGO and Virgo scientific collaboration, “Observation of gravitational waves from a binary black hole merger,” *Phys. Rev. Lett.* **116**, 061102 (Feb 2016).
- [2] A. Abramovici et al., “Ligo: The laser interferometer gravitational-wave observatory,” *Science* **256**(5055), 325–333 (1992).
- [3] F. Acernese et al., “Status of virgo detector,” *Classical and Quantum Gravity* **24**, S381–S388 (sep 2007).
- [4] G. Heinzl and C. Braxmaier et al., “Successful testing of the LISA technology package (LTP) interferometer engineering model,” *Classical and Quantum Gravity* **22**, S149–S154 (apr 2005).
- [5] M. Punturo et al., “The einstein telescope: a third-generation gravitational wave observatory,” *Classical and Quantum Gravity* **27**, 194002 (sep 2010).
- [6] eLISA Consortium and P. Amaro Seoane et al., “The Gravitational Universe,” *arXiv e-prints* , arXiv:1305.5720 (May 2013).
- [7] S. Barke and Y. Wang et al., “Towards a gravitational wave observatory designer: sensitivity limits of spaceborne detectors,” *Classical and Quantum Gravity* **32**, 095004 (apr 2015).
- [8] J. Y. Vinet, V. Brisson, and S. Braccini, “Scattered light noise in gravitational wave interferometric detectors: Coherent effects,” *Phys. Rev. D* **54**, 1276–1286 (Jul 1996).
- [9] S. Hild, *Beyond the first Generation: Extending the Science Range of the Gravitational Wave Detector GEO600*, PhD thesis, Von der Fakultat für Mathematik und Physik der Gottfried Wilhelm Leibniz Universität Hannover zur Erlangung des Grades (2007).
- [10] C. P. Sasso, G. Mana, and S. Mottini, “The LISA interferometer: impact of stray light on the phase of the heterodyne signal,” *Classical and Quantum Gravity* **36**, 075015 (mar 2019).
- [11] M. Lequime, V. Khodnevych, M. Zerrad, M. Lintz, and C. Amra, “Coherent detection of the light back-scattered by a rough surface,” in [*Optical Interference Coatings Conference (OIC) 2019*], *Optical Interference Coatings Conference (OIC) 2019* , TE.7, Optical Society of America (2019).
- [12] V. Khodnevych, S. Di Pace, J. Y. Vinet, N. Dinu-Jaeger, and M. Lintz, “Study of the coherent perturbation of a Michelson interferometer due to the return from a scattering surface,” in [*International Conference on Space Optics & ICSO 2018*], *Society of Photo-Optical Instrumentation Engineers (SPIE) Conference Series* **11180**, 111807T (July 2019).

- [13] B. P. Abbott and R. Abbott et al., “A guide to LIGO–virgo detector noise and extraction of transient gravitational-wave signals,” *Classical and Quantum Gravity* **37**, 055002 (feb 2020).
- [14] I. Khan, M. Lequime, M. Zerrad, and C. Amra, “Coherent detection of the light backscattered by an optical surface,” in [*International Conference on Space Optics ICSO 2020*], Cugny, B., Sodnik, Z., and Karafolas, N., eds., **11852**, 1185241, International Society for Optics and Photonics, SPIE (2021).
- [15] I. Khan, M. Lequime, M. Zerrad, and C. Amra, “Detection of ultralow light power back-reflected or back-scattered by optical components using balanced low-coherence interferometry,” *Phys. Rev. Applied* **16**, 044055 (Oct 2021).
- [16] C. Amra, M. Lequime, and M. Zerrad, [*Electromagnetic Optics of Thin-Film Coatings: Light Scattering, Giant Field Enhancement, and Planar Microcavities*], Cambridge University Press (2021).
- [17] I. Khan, M. Lequime, M. Zerrad, and C. Amra, “Characterization of light backscattered from optical components using balanced low coherence interferometry,” in [*Advances in Optical Thin Films VII*], Lequime, M. and Ristau, D., eds., **11872**, 118720S, International Society for Optics and Photonics, SPIE (2021).
- [18] M. Lequime and J. Lumeau, “Accurate determination of the optical performances of antireflective coatings by low coherence reflectometry,” *Appl. Opt.* **46**, 5635–5644 (Aug 2007).